Structure and RNA Interactions of the N-Terminal RRM Domains of PTB

Peter J. Simpson,[1,5] Tom P. Monie,[1,5]
Andrea Szendrői,[1] Natalia Davydova,[1]
Jonathan K. Tyzack,[1] Maria R. Conte,[2]
Christopher M. Read,[2] Peter D. Cary,[2]
Dmitri I. Svergun,[3,4] Peter V. Konarev,[3,4]
Stephen Curry,[1,*] and Stephen Matthews[1,*]
[1]Department of Biological Sciences
Imperial College
South Kensington Campus
Exhibition Road
London SW7 2AZ
United Kingdom
[2]Biophysics Laboratories
Institute of Biomedical and Biomolecular Sciences
University of Portsmouth
St. Michael's Building
Portsmouth PO1 2DT
United Kingdom
[3]European Molecular Biology Laboratory
Hamburg Outstation
EMBL c/o DESY
Notkestrasse 85
D-22603 Hamburg
Germany
[4]Institute of Crystallography
Russian Academy of Sciences
Leninsky pr. 59
117333 Moscow
Russia

Summary

The polypyrimidine tract binding protein (PTB) is an important regulator of alternative splicing that also affects mRNA localization, stabilization, polyadenylation, and translation. NMR structural analysis of the N-terminal half of PTB (residues 55–301) shows a canonical structure for RRM1 but reveals novel extensions to the β strands and C terminus of RRM2 that significantly modify the β sheet RNA binding surface. Although PTB contains four RNA recognition motifs (RRMs), it is widely held that only RRMs 3 and 4 are involved in RNA binding and that RRM2 mediates homodimerization. However, we show here not only that the RRMs 1 and 2 contribute substantially to RNA binding but also that full-length PTB is monomeric, with an elongated structure determined by X-ray solution scattering that is consistent with a linear arrangement of the constituent RRMs. These new insights into the structure and RNA binding properties of PTB suggest revised models of its mechanism of action.

*Correspondence: s.curry@imperial.ac.uk (S.C.); s.j.matthews@imperial.ac.uk (S.M.)
[5]These authors contributed equally to this work.

Introduction

Alternative splicing allows the production of multiple mRNA transcripts from a single pre-mRNA species and is a potent mechanism for generating eukaryotic protein diversity. Current estimates suggest that as many as 40%–60% of human genes contain alternatively spliced exons (Maniatis and Tasic, 2002). Exon choice is governed by a number of different factors such as the sequence and organization of 5′ and 3′ splice sites (and their associated branch points and pyrimidine tract), as well as positive and negative modulation of splice site strength by proteins which interact with specific sequences embedded in exons and introns (Maniatis and Tasic, 2002; Roberts and Smith, 2002; Wagner and Garcia-Blanco, 2001). The repression of exon inclusion is thus a key component of alternative splicing (Black, 2003), and in mammalian cells the 57 kDa polypyrimidine tract binding protein (PTB) has emerged as an important negative regulator of alternative splicing for over a dozen genes, including α- and β-tropomyosin (Mulligan et al., 1992; Pérez et al., 1997a; Singh et al., 1995), α-actinin (Southby et al., 1999), c-src tyrosine kinase (Chan and Black, 1997), and the γ2 subunit of the GABA$_A$ receptor (Zhang et al., 1999). PTB has also been implicated in the regulation of polyadenylation (Lou et al., 1999; Moreira et al., 1998), stabilization (Hamilton et al., 2003; Knoch et al., 2004; Tillmar and Welsh, 2002), and localization (Cote et al., 1999; Li and Yen, 2002) of mRNA. Further, the protein is recruited by the internal ribosome entry sites (IRESes) of a number of viral and cellular mRNAs to stimulate translation initiation (Hellen et al., 1993; Hunt and Jackson, 1999; Mitchell et al., 2003; Pilipenko et al., 2001).

These diverse activities are linked by the RNA binding specificity of PTB for short, single-strand pyrimidine motifs (e.g., UCUU, UCUUC, UUCUCU, CUCUCU) usually present in multiple, distributed copies within intron or IRES sequences (Chou et al., 2000; Kolupaeva et al., 1996; Pérez et al., 1997a; Pilipenko et al., 2001; Zhang et al., 1999). In alternative splicing, multiple copies of PTB are generally presumed to bind the RNA. They appear to act either by directly blocking binding of constitutive splicing factors (Charlet et al., 2002; Gromak et al., 2003a; Singh et al., 1995; Zhang et al., 1999) or by remodeling the RNA to "loop-out" control elements or whole exons which are then ignored by the splicing machinery (Chou et al., 2000; Liu et al., 2002; Wagner and Garcia-Blanco, 2001), though an interesting exception to this general rule has been reported (Gromak et al., 2003b). PTB has been shown to make multipoint contacts with IRES RNA and is proposed to have a chaperone function, stabilizing an active RNA conformation (Kaminski et al., 1995; Kolupaeva et al., 1996; Pilipenko et al., 2001). For example, in the case of the APAF-1 IRES, PTB alters the RNA structure to provide an entry point for the ribosomal 40S subunit (Mitchell et al., 2003).

PTB contains four RNA recognition motifs (RRMs), widely conserved structural domains that usually have
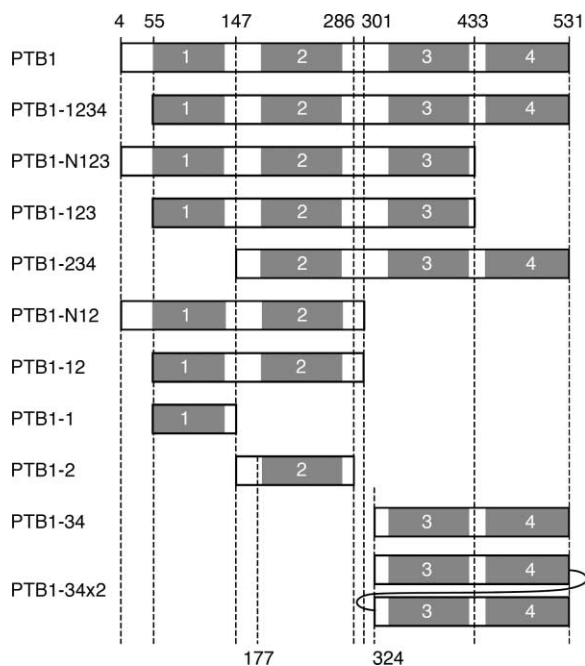
Figure 1. PTB Constructs Used in This Study

RRM domains are shaded gray. Construct boundaries are indicated by dashed lines; a dotted line indicates the N terminus resulting from proteolytic cleavage of PTB1-2.

$\beta\alpha\beta\beta\alpha\beta$ topology and fold to provide a four-strand β sheet surface for RNA binding. We previously solved the structure of the C-terminal domain (PTB1-34) which contains RRMs 3 and 4 and showed that the β sheet surfaces of both domains cooperate, along with the conserved linker that connects them, in binding RNA (Conte et al., 2000; Yuan et al., 2002). We present here the structure of the N-terminal half of the protein (PTB1-12), which contains RRMs 1 and 2; while RRM1 is canonical, RRM2—like RRM3—has a five-strand β sheet. Strikingly, we find that RRM2 exhibits an unprecedented configuration of RNP1 and RNP2 motifs. Contrary to previous reports (Bothwell et al., 1991; Kaminski et al., 1995; Oh et al., 1998; Pérez et al., 1997b), we also show that the N-terminal RRMs of PTB contribute substantially to RNA binding and that PTB is a monomer in solution. These results, which reveal new aspects of RRM adaptability and the structure and RNA binding activities of PTB, will impact models of the mechanism of action of the protein.

Results

NMR Analysis of PTB1-12

Initial NMR structural studies were carried out on PTB1-12 (residues 55–301), a fragment containing RRM domains 1 and 2 (Figure 1). NMR spectra recorded on a ~1 mM sample of PTB1-12 revealed relaxation properties consistent with protein aggregation (^{15}NH T$_2$ < 25 ms). Dilution to ~250 μM reduced the spectral line widths dramatically which, along with deuteration, allowed a complete sequential assignment of the two RRM regions (Simpson et al., 2002). The overall tumbling times for RRM1 (τ_c = 13.7 $\pm$ 0.7 ns) and RRM2 (τ_c = 16.1 $\pm$ 0.9

ns) in the diluted sample of PTB1-12 are significantly different, indicating that the two domains tumble independently and are unlikely to contact each other. Therefore, for high-resolution structure calculation we dissected PTB1-12 into two subfragments, PTB1-1 (residues 55–147) and PTB1-2 (residues 147–301), which incorporate RRM1 and RRM2, respectively (Figure 1). The NMR spectra for PTB1-1 are consistent with a soluble, monomeric domain. However, at millimolar concentrations, PTB1-2 displays NMR line widths comparable to the aggregated state of PTB1-12. Again, dilution to ~250 μM greatly reduced the self-association (e.g., ^{15}NH T$_2$ increased to ~65 ms), making comprehensive NMR studies feasible (see Supplemental Figure S1). Interestingly, the N terminus of PTB1-2 (residues 147–176), which corresponds to the polypeptide linker between RRMs 1 and 2, is susceptible to proteolysis. Once cleaved, the tendency for the isolated RRM to associate is abolished, (τ_c = 8.4 $\pm$ 0.5 ns) allowing high-quality NMR spectra to be recorded at millimolar concentrations. This suggests that the unstructured interdomain linker may mediate the nonspecific self-association observed for subfragments PTB1-12 and PTB1-2 (see below). NMR structure determination statistics are summarized in Table 1.

Solution Structure of PTB1-1

PTB1-1 is a canonical RRM with a four-strand β sheet backed by two helices (Figure 2A). The loop between helix α2 and strand β4 is extended by an additional β-hairpin, a feature observed previously in other RRMs (Xu et al., 1997) (Figure 3A). Intriguingly the C terminus of PTB1-1 lies across the top of the β sheet surface in an extended conformation that is similar to the corresponding feature in U1A, though in the latter case the chain is terminated by a short helix that has been shown to interact with RNA (Avis et al., 1996; Oubridge et al., 1994). In PTB1-1 the conformation of the C-terminal polypeptide is stabilized by hydrophobic contacts between L136 and a pocket formed by the side chains of V60, L89, and F98 and the aliphatic portions of N87 and E100 (Figure 3B), as evidenced by a number of NOEs between these residues.

The β sheet surface provides the central platform for RNA binding in this type of domain and frequently contains a triad of aromatic side chains that project from the RNP1 and RNP2 motifs on the central pair of strands (Birney et al., 1993). Two of these positions lie side-by-side on the adjacent strands and provide stacking interactions to orient the RNA ligand; in PTB1-1 these positions are occupied by H62 and F98 (Figure 3A). In addition, the surface is also populated by a number of basic and polar residues that could form specific hydrogen bond or salt bridge interactions with RNA bases or the sugar-phosphate backbone (see below).

Solution Structure of PTB1-2

In contrast to PTB1-1, the ^{15}N(H) heteronuclear NOE data indicate that regions in addition to the canonical RRM domain are highly structured (data not shown). The solution structure of PTB1-2 (Figure 2B) reveals that it is a five-stranded RRM with $\beta\alpha\beta\beta\alpha\beta\beta$ topology (Figure 3C).

Table 1. Structural Statistics

	$<\text{RRM1}>$[a]	RRM1$_{av\_min}$	$<\text{RRM2}>$[a]	RRM2$_{av\_min}$
Rmsd from experimental restraints				
Distance (Å)	0.018 ± 0.0022	0.013	0.009 ± 0.0011	0.006
Dihedral angle (°)	0.141 ± 0.0652	0.070	0.120 ± 0.0280	0.050
Rmsd from idealized covalent geometry				
Bonds (Å)	0.0013 ± 0.00010	0.0010	0.0008 ± 0.00010	0.00056
Angles (°)	0.286 ± 0.0105	0.268	0.254 ± 0.0039	0.243
Impropers (°)	0.157 ± 0.0186	0.133	0.104 ± 0.0078	0.088
XPLOR energies (kcal/mol)[b]				
Total	58.7 ± 7.2	42.6	42.7 ± 3.3	34.4
Distance restraints	16.7 ± 3.8	7.7	6.27 ± 1.6	3.0
Dihedral restraints	0.2 ± 0.1	0.0	0.1 ± 0.1	0.0
Bonds	2.4 ± 0.4	1.4	1.2 ± 0.3	0.5
Angles	32.0 ± 2.3	28.0	31.1 ± 1.0	28.5
Improper	2.8 ± 0.6	1.9	1.5 ± 0.2	1.1
van der Waals	5.4 ± 1.6	3.6	2.6 ± 0.8	1.3
Coordinate rmsd from mean structure (Å)				
Superimposed by res. in secondary structure (backbone/heavy)	0.38 ± 0.06/0.84 ± 0.08		0.44 ± 0.12/0.92 ± 0.12	
Superimposed by all residues[d] (backbone/heavy)	0.49 ± 0.09/1.00 ± 0.12		0.62 ± 0.07/1.10 ± 0.14	
Ramachandran plot[c]				
Residues in most-favored regions (%)	74.3	74.7	67.3	70.1
Residues in additionally allowed regions (%)	19.8	22.7	27.6	26.8
Residues in generously allowed regions (%)	4.4	0.0	4.5	3.1
Residues in disallowed regions (%)	1.4	2.7	0.6	0.0

[a] Refers to the ensemble of 15 structures.
[b] Default force constants were used (Schwieters et al., 2003).
[c] Structural quality was evaluated using PROCHECK-NMR (Laskowski et al, 1996).
[d] Superimposition excludes unstructured residues at the N- and C termini.

The elaboration to the canonical RRM structure in RRM2 consists of a linker from the C-terminal end of β4 to a fifth strand (β5) that lies anti-parallel to β2, similar to features first identified in RRM3 of PTB (Conte et al., 2000). As a result the β sheet face in PTB1-2 is extended by a short β-hairpin-like motif linking the end of the β4-β5 linker and strand β5. Residues in the region Y267-N269 are arranged as a "pseudo-sixth strand" antiparallel to β5, as evidenced by cross-strand-like NOEs and chemical shifts (e.g., low-field Hα shifts of 5.14 ppm [Y267] and 5.49 ppm [N269]). Interestingly, in addition to this motif, the polypeptide beyond the end of β5 folds back to make stable contacts with the β4-β5 linker, generating a feature not seen in RRM3 (Figures 3C and 3D). Hence, in comparison to RRM3, RRM2 is extended at the C terminus by a further ten structured residues that contribute to the globular domain.

Topologically, PTB1-2 most closely resembles PTB RRM3, but there are significant differences in β sheet twist, disposition of the helices and loop conformations. One of the most striking differences is in the β4-β5 loop: whereas in RRM3 this loop (17 residues) exhibits significant flexibility, in RRM2 it is significantly shorter (13 residues) and is closely associated with the top of the β sheet surface. The principal stabilizing contacts are between L263 and V265 from the β4-β5 loop and a hydrophobic pocket formed by side chains from V183, I214 and L225 together with the aliphatic portions of K212, Q227, S272, and D274 (Figure 3D).

As well as being broader than in most other RRM domains, the β sheet surface of RRM2 contains longer strands, particularly β1, β3, and β4. The extension of β1 results from a previously unsuspected insertion that displaces the RNP2 motif by two residues from its normal position. The RNP2 motif is a 6 residue signature of the RRM domain that contains hydrophobic residues
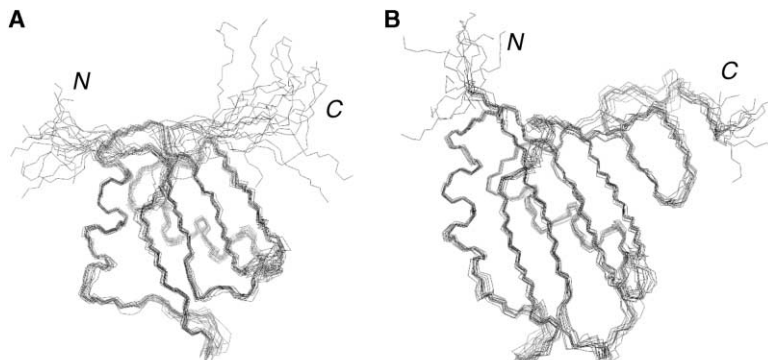

Figure 2. Solution Structures of PTB1 RRMs 1 and 2

(A) Family of the 15 lowest energy NMR structures of PTB1-1.
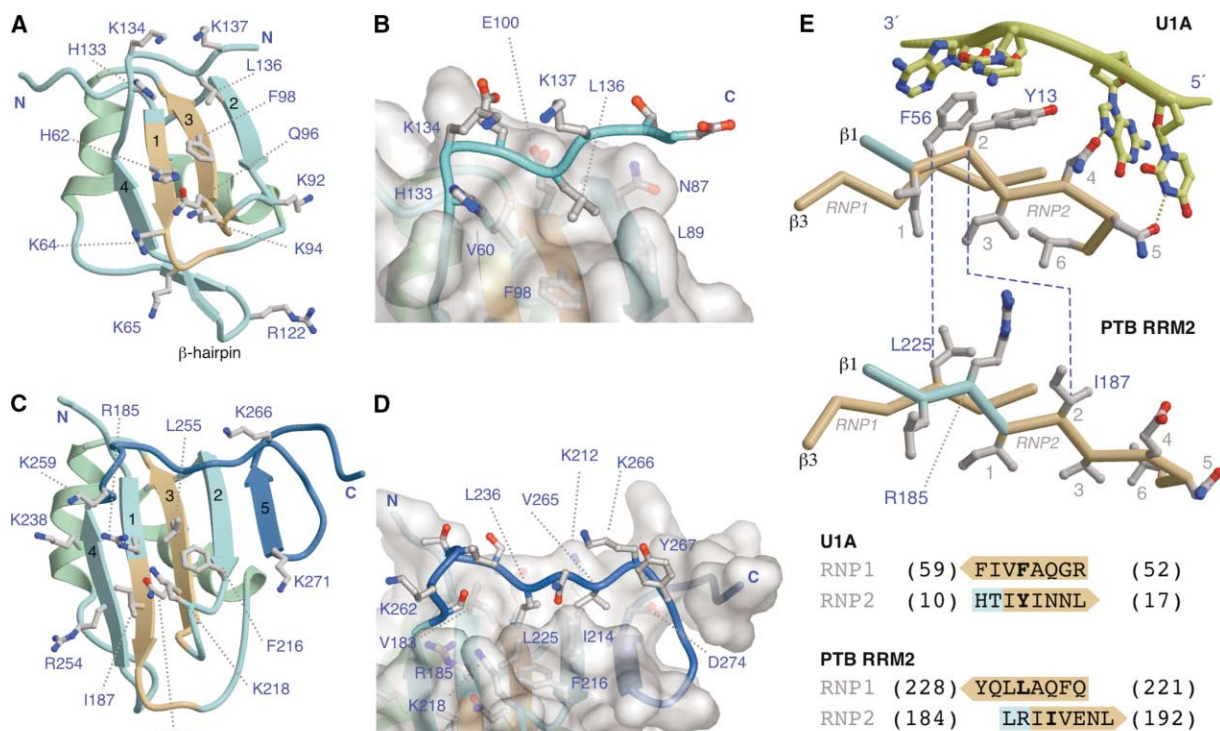(B) Family of the 15 lowest energy NMR structures of PTB1-2.

Figure 3. Three-Dimensional Structure of PTB RRMs 1 and 2

(A) Structure of PTB1-1. Helices are colored light green, the RNP motifs tan, and the remainder of the protein light blue. Selected side chains are indicated, color coded by atom type (gray, carbon; red, oxygen; blue, nitrogen). This color scheme is maintained in (B–E).
(B) Close-up view of the C-terminal peptide of PTB1-1 showing its interaction with the domain surface.
(C) Structure of PTB1-2. The C-terminal extension to the canonical RRM domain is colored dark blue.
(D) Close-up view of the C-terminal polypeptide of PTB1-2 showing its interaction with the domain surface.
(E) Structure and sequence comparison of RNPs of U1A (Oubridge et al., 1994) and PTB RRM2. Dotted lines indicate the relative shifts in PTB RRM2 of residues that are normally conserved as adjacent aromatic amino acids in RNP1 and RNP2. The top figure also shows how the RNP motifs of U1A coordinate interactions with a contiguous strand of RNA (yellow ribbon with ribose rings and bases shown in ball-and-stick). The sequences of the RNP motifs are shown at the bottom of the panel; in each case the RNP1 and RNP2 motifs are aligned as they occur in strands β3 and β1 of the relevant protein.

at positions 1, 3, and 6 which have their side chains buried in the core of the domain. The exposed positions within the motif provide coordinated interactions with a short contiguous segment of the RNA ligand. At positions 4 and 5, the RNP2 motif usually contains a pair of polar or glycine residues, both of which occur on the solvent side of the β sheet where they may make contact with bound RNA. The motif also normally possesses an aromatic residue at position 2 that is adjacent to a conserved aromatic residue at position 5 in the RNP1 motif located on the paired β3 strand; together these two aromatic sidechains provide base stacking interactions with consecutive RNA bases (Figure 3E). In PTB1-2 the normal configuration of RNP motifs is disrupted due both to the absence of the generally conserved aromatic residues and to the unprecedented shift in the relative positions of the motifs so that position 2 of RNP2 (I187) is adjacent to position 3 of RNP1 (Q223). These alterations to the canonical structure not only extend the β sheet RNA binding surface but also suggest that RRM2 may exhibit significantly altered coordination of its RNA ligand.

Dimerization

Although the NMR analyses revealed some aggregation behavior by PTB1-2, there was no strong indication of specific dimerization. We therefore reexamined the question of PTB homodimerization, in the first instance using size exclusion chromatography to investigate the association behavior of various subfragments. Full-length PTB1 migrated on the size exclusion column with an apparent molecular weight of 101 kDa, close to the 114 kDa observed previously (Pérez et al., 1997b) and significantly in excess of the molecular weight expected for a monomer (58.3 kDa) (Table 2). However, two strands of evidence suggest that the high apparent molecular weight is not due to dimerization. First, it is striking that the PTB1-1234 construct, which simply lacks the first 55 amino acids at the N terminus of the protein, migrates at 71 kDa, much closer to its theoretical value (52.5 kDa). Comparison of other PTB1 subfragments which differ only in whether or not they possess this 6 kDa N-terminal sequence shows that its presence is associated with an extra apparent molecular weight of 18–30 kDa (Table 2).

Table 2. Analysis of Molecular Weights of PTB Constructs

Construct	Theoretical MW (kDa)	Size Exclusion Chromatography		Analytical Ultracentrifugation	
		MW (kDa)	Ratio[a]	MW (kDa)	K_d (μM)[b]
PTB1	58.3	101	1.7	60.3 ± 2.4	M
PTB1-1234	52.5	71	1.4	53.7 ± 1.4	M
PTB1-N123	47.4	78	1.6	—	—
PTB1-123	41.6	51	1.2	Agg.	—
PTB1-234	42.3	56	1.3	Agg.	—
PTB1-N12	33.5	42	1.3	—	—
PTB1-12	28.3	24	0.92	27.1 ± 0.6	47 ± 12
PTB1-23	28.4	41	1.4	28.7 ± 0.1	15 ± 5
PTB1-1	11.7	—	—	12.8 ± 0.6	>1000
PTB1-2	12.8[c]	—	—	12.3 ± 0.6	95 ± 33
PTB1-34	23.1	22	1.0	20.1 ± 1.3	M
PTB1-34x2	47.0	49	1.0	—	—

[a] Ratio of MW measured by gel filtration to theoretical MW.
[b] Dissociation constant for dimerization; M indicates that a monomeric model gave the best fit to the data.
[c] Molecular weight for construct following proteolysis which reduced the domain to residues 177–284.

Second, the use of size exclusion chromatography to determine molecular weights depends on the assumption that the test protein is as globular as the protein standards used for column calibration: proteins with asymmetric proportions tend to migrate with anomalously high molecular weights (le Maire et al., 1980). We used small angle X-ray scattering to investigate the low-resolution structure of full-length PTB (Experimental Procedures; Figure 4A). The estimated molecular weight (55 ± 5 kDa) and the excluded particle volume (120 ± 10 nm³) both indicate that PTB1 is monomeric in solution. Moreover, the values of the maximum dimension of the molecule (D_{max} = 14 ± 1 nm) and the radius of gyration (R_g = 4.1 ± 0.1 nm) suggest that PTB1 is a rather elongated particle and this is corroborated by the profile of the distance distribution function $p(r)$ (Figure 4A, inset) (Feigin and Svergun, 1987) which is consistent with a cross-sectional diameter for PTB1 of around 3 nm. Re-
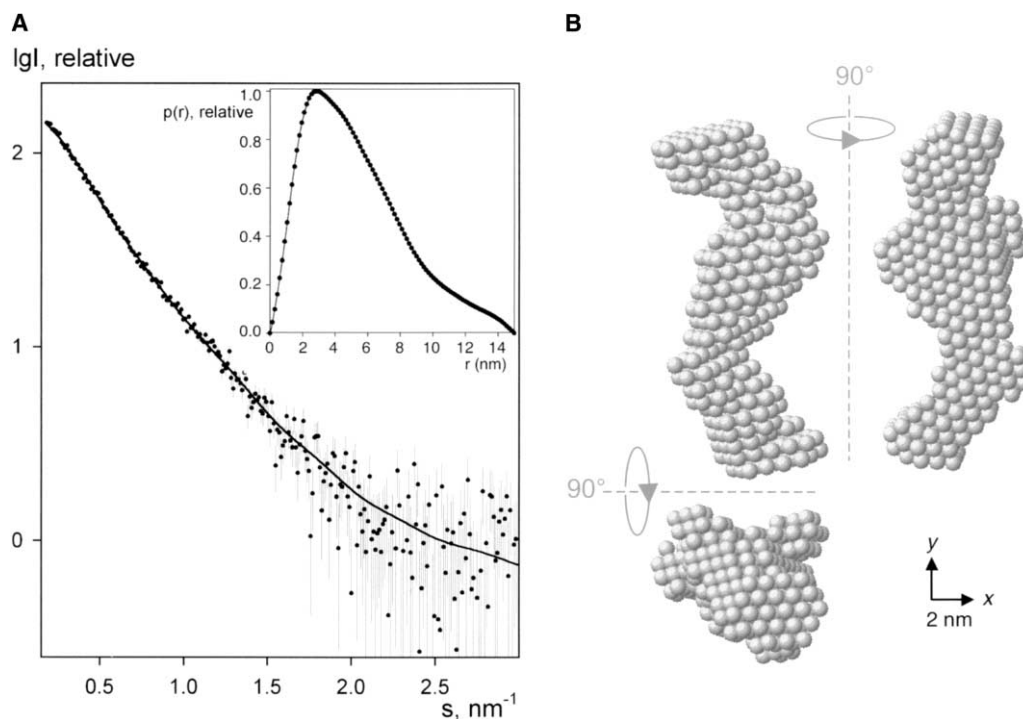

Figure 4. Small Angle X-Ray Scattering Analysis of the Conformation of Full-Length PTB

(A) Experimental X-ray scattering pattern from full-length PTB1 (dots with error bars) and the scattering computed from the typical ab initio model corrected for the constant term due to the contribution from the internal structure (full line). The distance distribution function is displayed in the insert.

(B) Typical low-resolution model of PTB1 restored ab initio by DAMMIN. Right and bottom views are rotated counterclockwise by 90° around y and x axes, respectively. The models were displayed using the program MASSHA (Konarev et al., 2001).
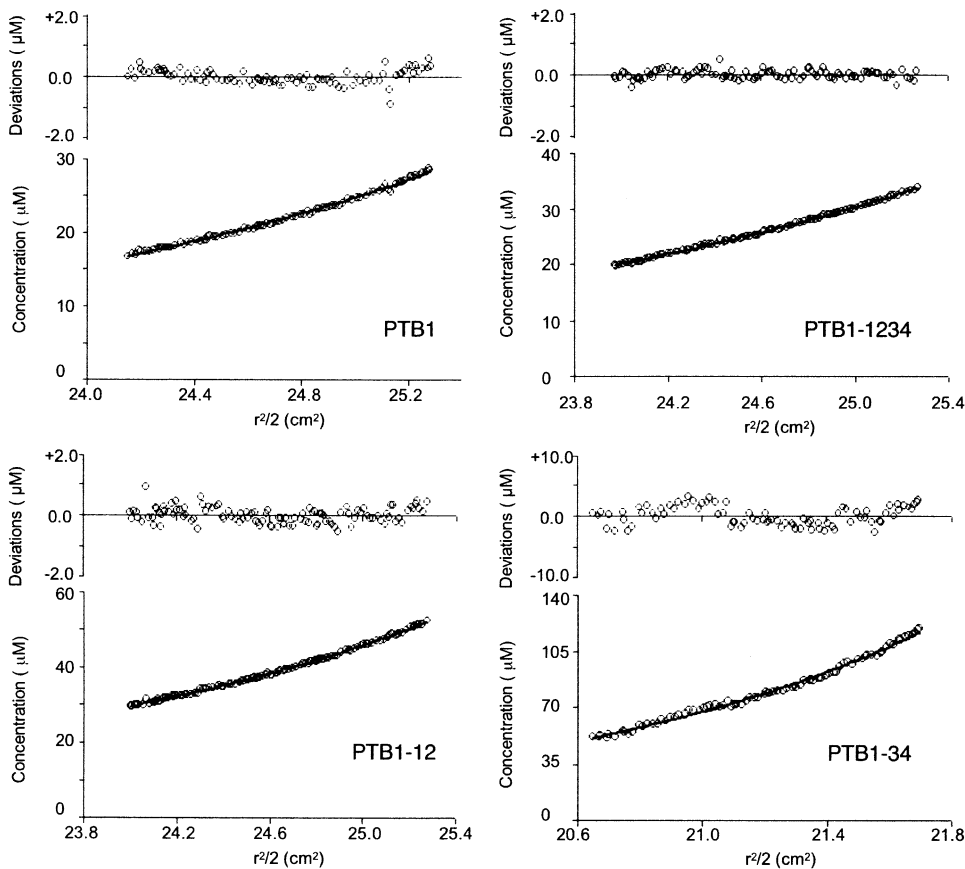
Figure 5. Representative Sedimentation Equilibrium Analytical Ultracentrifugation Data for PTB Constructs

Plots represent fitted data and deviations to either a single-species model (PTB1, PTB1-1234, PTB1-34) or a monomer-dimer model (PTB1-12) at the following run speeds and initial protein concentrations (PTB1: 8,000 rpm, 21.3 μM; PTB1-1234: 8,000 rpm, 21.8 μM; PTB1-12: 10,000 rpm, 35 μM; PTB1-34: 18,000 rpm, 100 μM).

construction of the particle reveals an elongated shape with a developed domain structure, which suggests a linear arrangement of the constituent RRM domains. In summary, not only do the SAXS data support the notion that the protein is monomeric in solution but they also suggest that the elongated proportions of PTB contribute to the overestimation of the molecular weight by size exclusion chromatography.

We also examined the association behavior of PTB using equilibrium sedimentation analytical ultracentrifugation (AUC) (Laue, 2001). In these experiments, the molecular weights determined for PTB1, PTB1-1234, and PTB1-34 were close to their theoretical monomeric values (Table 2; Figure 5). In contrast however, PTB1-2, PTB1-12, and PTB1-23 all returned apparent molecular weights in excess of their theoretical values if assumed to be monomeric. In each of these cases the best fit to the sedimentation profile was obtained by modeling the association behavior as a monomer-dimer equilibrium with dissociation constants (K_d) in the range 15–94 μM (Table 2). Overall the AUC data are consistent with the aggregation observed in NMR experiments involving subfragments of PTB that are truncated on either side of RRM2. Taken together, our biophysical analyses suggest that full-length PTB1 is a monomer in solution but

that fragmentation can lead to nonspecific aggregation, perhaps due to the exposure of hydrophobic surfaces that are normally masked within the intact protein.

RNA Binding

It is widely asserted that the dominant RNA binding activity of PTB is associated with RRMs 3 and 4, a notion based largely on data from UV crosslinking assays (Charlet et al., 2002; Kaminski et al., 1995; Oh et al., 1998; Pérez et al., 1997b). However, our RNA binding experiments do not support this view. We first used filter binding assays to investigate the binding of PTB1, PTB1-12, and PTB1-34 to intron and IRES RNA targets (Experimental Procedures). As expected, the full-length protein (PTB1) exhibited high affinity for both RNA targets. However, surprisingly, PTB1-12 appeared to bind RNA consistently tighter than PTB1-34 (Figure 6A).

Complexes of PTB with encephalomyocarditis virus (EMCV) IRES RNA were further analyzed in electromobility shift assays (EMSAs). Again it is evident that while PTB1 binds tightest, PTB1-12 binds with significantly higher (2- to 4-fold) affinity than PTB1-34 (Figure 6B). This pattern of behavior was also observed in EMSAs performed on complexes of PTB1-12 and PTB1-34 with RNA derived from PTB binding sites within the c-src
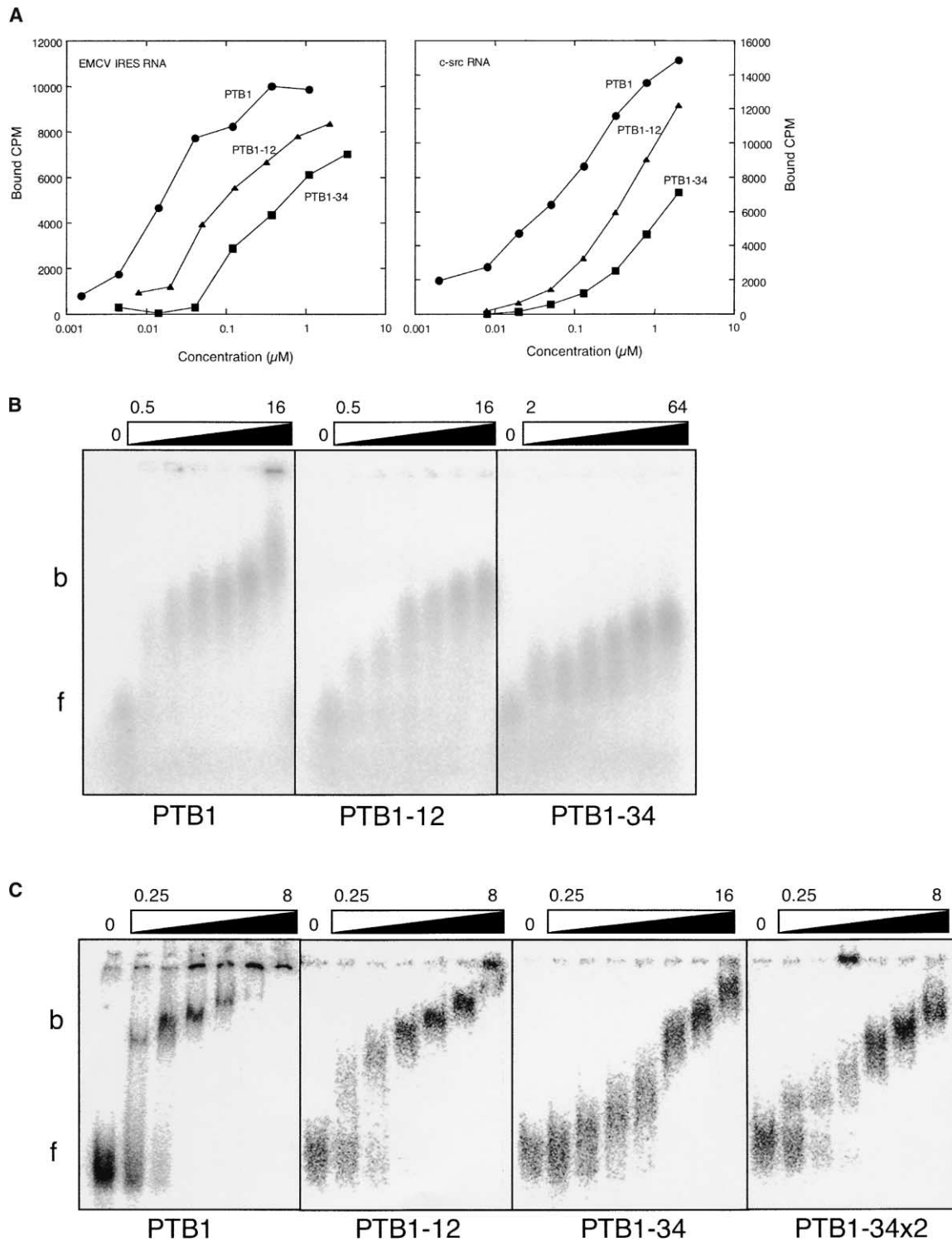
A

B

C

Figure 6. Analysis of RNA Binding by PTB and Selected Subfragments

(A) Filter binding assays.

(B) Agarose gel mobility shift assays with EMCV IRES RNA.

(C) Acrylamide gel mobility shift assays with c-src RNA. For (B) and (C), protein concentration increases in 2-fold steps; the highest and lowest concentrations in μM are indicated above each gel.

intron (Chou et al., 2000) (Figure 6C). Thus, for two dissimilar RNA targets we find that PTB1-12 binds with higher affinity than PTB1-34. In the context of the whole protein, it is therefore likely that all four RRMs contribute to high-affinity binding which explains why the subfragments bind with lower affinity. This notion is supported
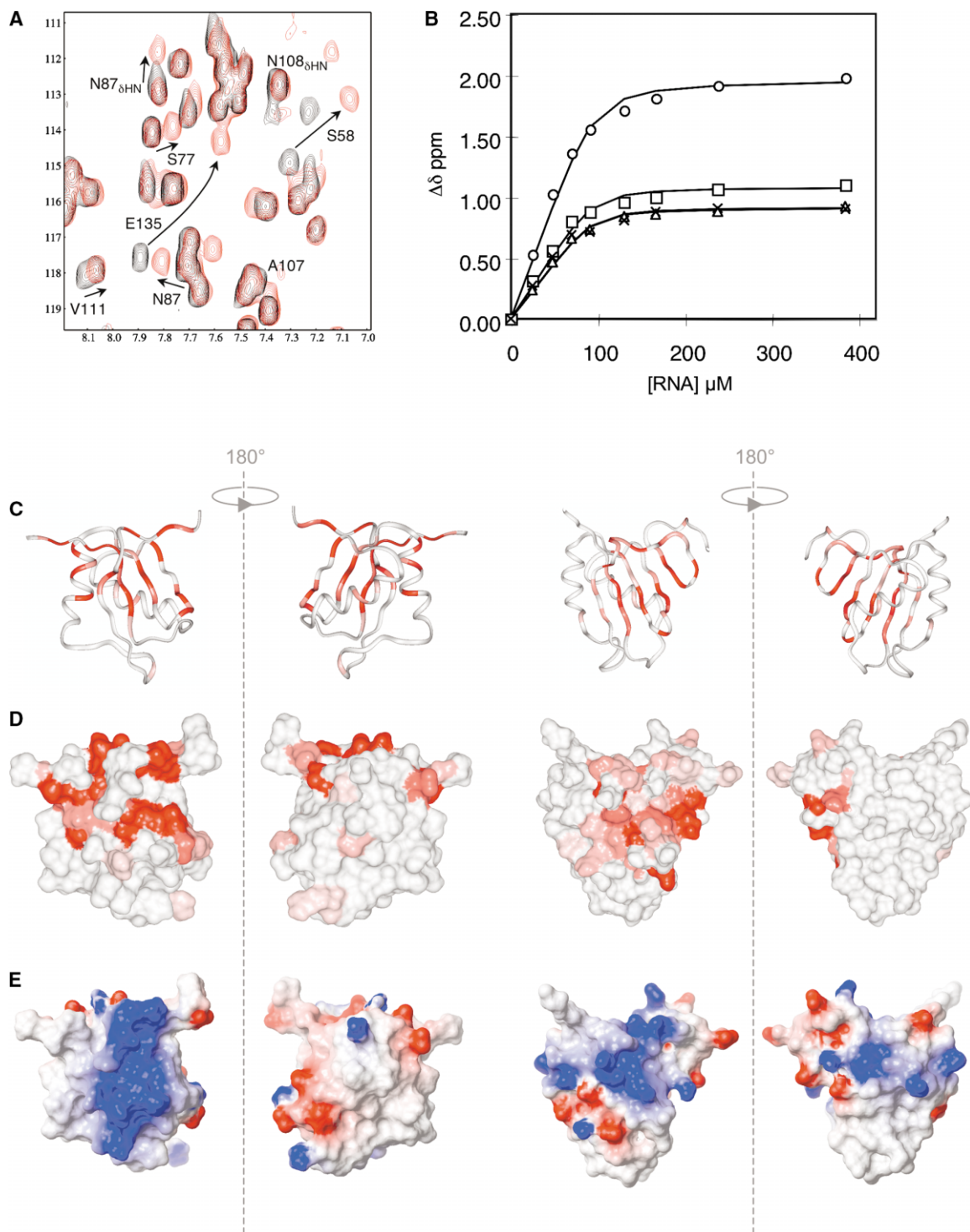
Figure 7. Chemical Shift Analysis of RNA Binding

(A) Region of the ^{1}H-^{15}N HSQC spectrum of PTB1-1 showing selected amide shift changes in the absence (black) and presence (red) of 4.75 equivalents of CUUCUCUCU.

(B) Representative binding isotherms determined from fitting the change in NMR chemical shift with ligand concentration of a number of PTB1-2 amide peaks. Key: circles, A224; squares, N220; crosses, T215; triangles, L263.

(C) Chemical shift mapping onto ribbon representations of PTB1-1 and PTB1-2. Residues are colored based on the magnitude of shift changes upon ligand binding ramped white (no significant change or could not be measured) to red (largest shift change).

(D) Surface representation of the data presented in (C).

(E) Electrostatic potential surfaces of PTB1-1 and PTB1-2; acidic and basic regions are colored red and blue respectively. Structures in (C)–(E) are shown in the same orientation.

by experiments which showed that binding of EMCV IRES RNA to full-length PTB1 protected the RRM1-RRM2 and the RRM3-RRM4 linker polypeptides from trypsin proteolysis (Supplemental Figure S2); these experiments also suggest that the RRM domains of PTB may operate as tandem pairs, as has been found for other RRM proteins such as sex-lethal (Handa et al., 1999).

NMR Mapping of RNA Binding Sites in PTB1-12

To further investigate the binding of RNA to PTB1-12, ^{15}N-labeled proteins were titrated with the RNA oligonucleotide CUUCUCUCU and monitored using 2D ^{1}H-^{15}N HSQC spectra (Figures 7A and 7B). This oligonucleotide corresponds to a PTB binding site that is present in duplicate in the c-src RNA transcript used in our RNA binding assays (Chou et al., 2000). Due to overlap in the 2D NMR spectrum of PTB1-12, most titrations were carried out with the single domain constructs PTB1-1 and PTB1-2. For both domains the chemical shift changes upon addition of RNA confirm that the β sheet surfaces, which are associated with the most basic patches on the protein, provide the principal RNA binding sites (Figures 7C–7E). In PTB1-2, chemical shift changes are observed across the entirety of the extended β sheet surface, with some of the most significant changes apparent in residues in and around the additional strand β5. Hence the RNA binding surface of PTB1-2 is extended significantly in comparison to both a canonical RRM domain and to the surface mapped in PTB1 RRM3 (Yuan et al., 2002). In addition, small shifts are observed in the C-terminal extension that bends back into an arrangement approximately antiparallel with the "pseudo sixth strand" implying that this region may also interact with RNA. Further shift perturbations are observed in the majority of residues in the β4-β5 loop that extends over the RNP motifs, suggesting that this region is intimately involved in ligand binding. This loop contains several residues which could contact RNA via electrostatic (K259, K266) or aromatic stacking (Y267) interactions.

In PTB1-2 the pattern of shift changes is consistent with RNA binding across the five-stranded β sheet in the shallow, concave face formed by the surface of the sheet and β4-β5 loop (Figures 7C and 7D). In PTB1-1, however, the pattern of shift changes is strikingly different. First, addition of RNA has a much more dramatic effect on the HSQC spectrum of PTB1-1, with ^{15}N chemical shift differences of up to almost 5 ppm observed in some backbone amide peaks (Figure 7A). Second, significant perturbations are observed not only in residues proximal to the RNP motifs but also at the N terminus of the RRM and on one face of helix 2, suggesting that the mode of RNA binding may differ significantly from RRM2 (Figures 7C and 7D). The largest changes in the HSQC spectrum are in the C-terminal region of PTB1-1 which lies on top of the β sheet and forms the beginning of the interdomain linker. The magnitude and extent of these shifts imply a significant conformational change upon RNA binding, perhaps indicative of displacement of the C terminus allowing the RNA increased access to the β sheet.

Titration of ^{15}N-labeled PTB1-12 with the same RNA oligonucleotide (CUUCUCUCU) revealed a pattern of chemical shift perturbations entirely consistent with those observed for the individual domains. Furthermore, the estimated dissociation constant for the PTB1-12/RNA interaction is comparable to those measured for the individual domains (K_d ∼5–10 μM), suggesting that each RRM may bind a separate RNA oligonucleotide. However, it remains possible that the two RRMs cooperate in binding to larger RNA ligands.

Discussion

PTB Structure and the Versatility of RRM Domains

This report provides new insights into the structure of the N-terminal RRM domains of PTB. RRM1 has a canonical structure for this type of domain, whereas RRM2 reveals itself to be a new and unexpectedly large variant on the RRM theme. It possesses a five-strand β sheet with a β4-β5 linker that is intimately associated with the upper portion of the β sheet RNA binding surface. Furthermore, RRM2 has a completely unprecedented configuration of RNP motifs that is likely to alter the disposition of bound RNA. Sequence comparisons indicate that all the novel features identified here in PTB RRM2 are conserved in PTB orthologs (Wagner and Garcia-Blanco, 2001), paralogs (Gooding et al., 2003), and homologs such as hnRNP-L (data not shown). Together with our previous reports on the C-terminal RRM domains of PTB (Conte et al., 2000), this study provides a detailed picture of the domain structure of PTB that will aid future experiments to dissect its function.

All RRMs of PTB Contribute to RNA Binding

The observations from NMR chemical shift analyses, filter binding, and electromobility shift assays all demonstrate that the N-terminal RRM domains of PTB contribute significantly to RNA binding. Indeed we found that PTB1-12 generally has a somewhat higher affinity for intron and IRES RNA targets than does PTB1-34, and we conclude that PTB interactions with RNA are likely to involve all four RRM domains of the protein. At first sight these findings appear to be at odds with the widely held view that the C-terminal RRM domains of PTB possess the dominant RNA binding activity (Charlet et al., 2002; Hamilton et al., 2003; Kaminski et al., 1995; Kolupaeva et al., 1996; Oh et al., 1998; Pérez et al., 1997b). However, this perception derives from the consistent observation that these domains do not efficiently UV crosslink to RNA targets (Charlet et al., 2002; Kaminski et al., 1995; Oh et al., 1998; Pérez et al., 1997b). Although UV crosslinking is a sensitive technique for detecting protein-RNA contacts, it cannot report on binding affinity. Where efforts have been made to obtain affinity measurements, for example using competition binding experiments (Kaminski et al., 1995; Pérez et al., 1997b) or gel mobility shift assays (Liu et al., 2002), the results have shown significant RNA binding activity in the N-terminal half of the protein, consistent with the findings presented here. We therefore believe there is a compelling case for embracing the notion that all four RRM domains of PTB are involved in interactions with RNA.

PTB Is a Monomer in Solution

Although gel filtration analysis indicates that PTB migrates at close to the molecular weight expected for a homodimer (Table 2) (Pérez et al., 1997b), SAXS (Figure 4) and AUC (Figure 5) data consistently indicate that the protein is monomeric in solution. Moreover, the elongated rod-like shape of the protein determined by SAXS (Figure 4B) provides a plausible explanation for the anomalously high protein molecular weight determined by gel filtration.

We did observe weak and nonspecific aggregation of PTB fragments incorporating RRM2, and we therefore suggest that previous reports of PTB self-association using deletion mutagenesis, which are often cited as support for dimerization of the protein, are probably also due to nonspecific interactions. For example, a study using SDS-PAGE analysis of chemical crosslinking of PTB found that, although most of the protein appeared monomeric, a very small proportion migrated at the weight expected for a dimer (Oh et al., 1998). The same study went on to show that PTB(169-293), which contains RRM2 in its entirety, formed a significantly greater proportion of dimeric and trimeric species, and this was interpreted as evidence that RRM2 is principally responsible for mediating self-association. However, these crosslinking data are consistent with our observation that removal of domains from either side of RRM2 promotes nonspecific aggregation, perhaps by exposing hydrophobic surfaces that are buried within the intact protein. In a different approach, pull-down experiments using a GST-PTB fusion protein to capture a range of PTB fragments found only a weak interaction with full-length PTB but much stronger interactions with fragments containing RRM2 and at least one other RRM domain (Pérez et al., 1997b). Although these results were also interpreted as evidence that RRM2 promotes dimerization, they are again consistent with the idea that fragmentation promotes nonspecific self-association. In particular, the fact that a strong interaction was found between GST-PTB and PTB(1-264)—a subfragment that we now know has an incomplete and therefore probably unstructured RRM2 domain—underscores the likelihood that the technique was detecting nonspecific interactions. Finally, yeast two-hybrid experiments which demonstrated self-association linked to the N-terminal half of PTB (Oh et al., 1998) cannot exclude the possibility that the interaction is nonspecific or perhaps mediated by interactions with RNA.

New Models of PTB Function

The findings reported here have significant implications for possible models of PTB action. PTB makes multipoint interactions with RNA in binding to intron and IRES targets (Chou et al., 2000; Kolupaeva et al., 1996; Pilipenko et al., 2001; Wagner and Garcia-Blanco, 2001; Zhang et al., 1999), and it now appears that these involve all four RRM domains of the protein so that PTB-RNA interactions are likely to be highly cooperative. PTB has also been proposed to bind in multiple copies to effect negative regulation of alternative splicing or stimulation of IRES-dependent translation initiation and the assumption that it is dimeric has often been incorporated implicitly or explicitly into models of action (Chou et al., 2000; Hamilton et al., 2003; Kaminski and Jackson, 1998; Kolupaeva et al., 1996; Liu et al., 2002; Wollerton et al., 2004). For example, in the case of alternative splicing it has been proposed that PTB dimers may mediate the "crosslinking" of binding sites that are widely separated in the pre-mRNA so as to loop out whole exons or key control elements, thus leading to exon silencing (Wagner and Garcia-Blanco, 2001). Our finding that PTB is monomeric in solution suggests that PTB dimerization may not be involved in this process. For example it is conceivable that that a single PTB monomer could crosslink distal binding sites, with the N-terminal RRMs binding to one site and the C-terminal RRMs binding to another, a model which assumes the RRMs act as tandem pairs and is supported by the RNA-mediated protection of the RRM1-RRM2 and RRM3-RRM4 polylinkers (see Supplemental Data). Alternatively, it may be that RNA binding or association with other proteins may induce conformational changes in PTB that reveal an interface for dimerization. Although there is no direct evidence for RNA-induced dimerization from our titration experiments with PTB1-12 and the oligonucleotide CUUCU CUCU, larger protein and RNA constructs may be required to reveal such activity.

Experimental Procedures

Plasmid Construction

PTB1 and all PTB subfragments (Figure 1) were subcloned by PCR using oligonucleotides that introduced a 5′ BamHI site and a 3′ HindIII site to allow ligation of the digested PCR product into plasmid pQE9 (Qiagen). This adds a noncleavable N-terminal MRGSHH HHHHGS tag (the codons for the second GS dipeptide in this tag correspond to the 5′ BamHI site). The construct pQE9-PTB1-34x2 comprises PTB1(337-531) and PTB1(326-531) separated by a GS dipeptide within the same open reading frame and thus contains two copies of RRMs 3 and 4 within a single polypeptide.

A plasmid for generation of an RNA transcript corresponding to the PTB binding sites within the intron upstream of the N1 exon of c-src (Chou et al., 2000) was generated using a complementary pair of DNA oligonucleotides designed to generate sticky ends corresponding to 5′ HindIII and 3′ EcoRI restriction sites upon hybridization; this allowed ligation into pGEM-4Z downstream of the T7 promoter to generate pGEM-4Z-c-src which produces an 88 nt RNA transcript: 5′-<u>GGGAGACAAGCUUC</u>GAAUUGGGUACGGCCCUGUC UUCGCACCUC<u>AG</u>CCUCUCCUUCUCUCUGCUUCUCUCUCGCUG GCCCUUA<u>GAAUU</u> (underlining indicates 5′ vector sequence, the intron branch point, and the 3′ vector sequence, respectively).

Protein Expression and Purification

Proteins were expressed in SG13009 *E. coli* and purified on TALON resin (Clontech) essentially as described previously (Conte et al., 2000). PTB1, PTB1-1, and PTB1-2 samples were further purified by size exclusion chromatography using a Superdex 200 HR 10/30 column at a flow rate of 0.5 ml/min prior to AUC analysis. For SAXS experiments, PTB1 also underwent ion exchange on a POROS HS50 column.

Samples for NMR were also purified by ion exchange before concentration in 5 kDa MWCO Vivaspin-20 centrifugal concentrators and buffer exchanged into 50 mM sodium phosphate buffer, pH 6.5, 100 mM NaCl, 10 mM DTT, 2 mM NaN$_3$. Final sample concentrations were 1 mM PTB1-1, 0.3 mM PTB1-2 (0.1 mM for ^{15}N relaxation), and 0.2 mM PTB1-12. Despite purification, the PTB1-2 sample (PTB residues 147–285) used for NMR suffered proteolysis that removed the unstructured N-terminal peptide and one residue at the C terminus, leaving a stable fragment, PTB(177-284), with enhanced solubility.

NMR Spectroscopy

NMR spectra were recorded at 303 K (310 K for PTB1-2) on a 500 MHz four-channel Bruker DRX500 spectrometer equipped with a z-shielded gradient triple resonance cryoprobe. Sequence-specific backbone assignments for PTB1-12 were determined previously (Simpson et al., 2002). Side chain assignments were obtained from HCCH-TOCSY experiments (Bax et al., 1990), aided by the 3D NOESY spectra and an (HB)CB(CGCD)HD for aromatic residues (Yamazaki et al., 1993). 3D ^{1}H-^{15}N (500 MHz) and ^{1}H-^{13}C NOESY-HSQC (800 MHz) spectra provided distance restraints. Spectra were processed with NMRPipe (Delaglio et al., 1995) and analyzed using NMRView (Johnson and Blevins, 1994).

Structure Calculation

A total of 1800 and 2670 NOEs were assigned in spectra of PTB1-1 and PTB1-2, respectively. From these, 906 (PTB1-1) and 1490 (PTB1-2) distance restraints were derived for the final structure calculations. For PTB1-1 this comprised 196 long-range (i to i > 4), 99 medium-range (1 < i ≤ 4), 221 sequential, 248 intramolecular, and 142 ambiguous NOEs. For PTB1-2 this comprised 316 long-range, 160 medium-range, 328 sequential, 428 intramolecular, and 258 ambiguous NOEs. 58 (66) distance restraints for 29 (33) hydrogen bonds were also included for PTB1-1 (PTB1-2). For PTB1-1, distance restraints were supplemented with 113 dihedral angles, comprising 96 TALOS-based backbone dihedrals (Cornilescu et al., 1999) and 17 χ^1 ranges derived from NOE patterns and consideration of initial structures. 151 dihedrals (112 backbone, 39 χ^1) were obtained for PTB1-2. This amounts to an average of 13.5 and 16.7 restraints per residue for the two structured RRM regions of PTB1-12. Structure calculations used a hybrid distance geometry/simulated annealing protocol implemented in Xplor (Schwieters et al., 2003). No distance violation greater than 0.5 Å or dihedral violation greater than 5° were tolerated in the final ensemble. Structural coordinates have been deposited in the PDB (ID codes 1SJQ and 1SJR).

^{15}N Relaxation Measurements

^{15}N T_1, ^{15}N T_2, and ^{1}H-^{15}N heteronuclear NOE data were measured essentially as described elsewhere (Farrow et al., 1994; Kay et al., 1989). For T_1 and T_2 measurements a range of relaxation delays up to 1500 and 200 ms were employed, respectively. Relaxation curves were characterized by seven to eight time points with one to two duplications.

Chemical Shift Assays

For NMR mapping experiments, ^{15}N-labeled protein (50–100 μM) was titrated with RNA dissolved in identical buffer solution at a concentration of 1–4 mM. 2D ^{15}N-^{1}H HSQC spectra were recorded at a range of ligand:protein molar ratios up to 4.75, 5.0, and 4.0 equivalents for PTB1-1, PTB1-2, and PTB1-12, respectively. Amide peak shift changes were judged to be significant using a plot of Δδ(^{1}H) versus Δδ(^{15}N) as described (Williamson et al., 1997) and ranked using a weighted sum of the ^{1}H and ^{15}N shift changes (Wishart et al., 1991).

RNA Transcription and Binding Assays

EMCV IRES (563 nt) and c-src intron (88 nt) RNA transcripts were transcribed in the presence of [α-^{32}P] UTP, by T7 RNA polymerase from 1.0 μg of either BglII linearized pGEMSG6A (Kaminski et al., 1994) or EcoRI linearized pGEM4-Z-c-src respectively. The template was digested by DNaseI and the RNA purified on a spin column (G-25 Microspin; Amersham-Pharmacia), ethanol precipitated and resuspended in diethylpyrocarbonate-treated water. Prior to use in binding assays, the RNA was refolded by heat denaturation for 5 min at 70°C followed by cooling to room temperature. Filter binding assays were performed as described previously (Conte et al., 2000). For gel shift assays 1.0 nM EMCV IRES RNA and 3.4 nM c-src RNA were incubated for 10 min at room temperature with various concentrations of PTB proteins. Final reaction conditions were 10 mM HEPES (pH 7.2) (substituted with 10 mM Tris [pH 8.0] for the c-src RNA), 3 mM MgCl$_2$, 5 mM DTT, 100 mM KCl, 50 μg/ml tRNA, 40 μg/ml HSA, 5% glycerol. 2 μl native loading buffer (50% glycerol, 0.01% bromophenol blue) was added and the samples loaded into either a 1.0% 1× TB (89 mM Tris-borate) agarose gel (EMCV IRES RNA) or a prefocused 0.5× TBE (1× TBE is 89 mM Tris-borate, 2 mM EDTA) 8% native polyacrylamide gel (c-src RNA). Agarose gels were run at room temp for 90 min at 60 V, acrylamide gels for 25 min at 300 V and 4°C. Dried gels were analyzed on a Fuji BAS3000 phosphoimager.

Analytical Ultracentrifugation

Low-speed sedimentation equilibrium experiments were performed on a Beckman XL-A analytical ultracentrifuge. Samples were loaded into six-channel epon charcoal-filled centerpieces in an eight-position AN50Ti rotor. The optical pathlength was 12 mm. Sample absorbance at 280 nm was scanned stepwise in 0.001 cm increments with five replicates. Protein concentrations in the range 21–205 μM in 25 mM Tris, 250 mM NaCl, 2 mM DTT (pH 7.2) were centrifuged to equilibrium (15–24 hr) at 4°C using run speeds from the range 8,000, 10,000, 18,000, 22,000, 24,000, 35,000, and 36,000 rpm based on molecular weight. A radial calibration of the rotor was carried out at 3,000 rpm. Partial specific volumes and buffer density values at 4°C were computed using the program Sednterp. For each protein, data sets from at least four different speeds were simultaneously fitted to ideal single-species and to monomer-dimer models using WinNonLin (Version 1.06) and Beckman Optima XL-A/XL-1 data analysis software (version 4.0).

Size Exclusion Chromatography

Size exclusion chromatography was run on a Superdex 200 HR 10/30 column equilibrated with 25 mM Tris, 250 mM NaCl, 2 mM DTT, pH 7.2. Protein samples (at up to ~400 μM in running buffer) were applied at a flow rate of 0.5 ml/min. A standard curve was generated using molecular weight markers (Sigma-Aldrich) applied at a stock concentration of 6.25 mg/ml.

SAXS Experiments and Data Processing

The synchrotron radiation X-ray scattering data were collected on the X33 camera at the EMBL on the storage ring DORIS III (DESY, Hamburg). The scattering intensity patterns $I(s)$ at protein concentrations of 3.4, 6.7, 10, and 20 mg/ml were recorded at a sample-detector distance of 2.4 m covering the range of momentum transfer $0.15 < s < 3.5$ nm^{-1} ($s = 4\pi \sin(\theta)/\lambda$, where 2θ is the scattering angle and $\lambda = 0.15$ nm is the X-ray wavelength). The data were collected in 15 successive 1 min frames to check for radiation damage and processed using the program package PRIMUS (Konarev et al., 2003).

The maximum particle dimension D_{max} was estimated using the orthogonal expansion program ORTOGNOM (Svergun, 1993). The forward scattering $I(0)$ and the radius of gyration R_g were evaluated using the Guinier approximation assuming that at very small angles ($s < 1.3/R_g$) the intensity is represented as $I(s) = I(0) \exp(-(sR_g)^2/3)$. These parameters were also computed from the entire scattering patterns using the indirect transform package GNOM (Svergun, 1992), which also provides the distance distribution function $p(r)$ of the particle. The molecular mass of the solute was evaluated by comparison with scattering from a reference solution of BSA (66 kDa). The excluded volume of the hydrated particle V (Porod volume) was computed from the data after appropriate constant subtraction to force the s^{-4} decay of the intensity at higher angles. For globular proteins, V in nm^3 is about twice the mass in kilodaltons. A low-resolution model of full-length PTB1 was constructed using the ab initio program DAMMIN (Svergun, 1999).

Supplemental Data

The Supplemental Data are available at http://www.structure.org/cgi/content/full/12/9/1631/DC1 and include additional details of the sample conditions used to minimize protein aggregation in the structure determination of PTB1-2 and a protease protection experiment to probe the impact of RNA binding on full-length PTB.

References

Avis, J.M., Allain, F.H., Howe, P.W., Varani, G., Nagai, K., and Neu-haus, D. (1996). Solution structure of the N-terminal RNP domain of U1A protein: the role of C-terminal residues in structure stability and RNA binding. J. Mol. Biol. *257*, 398–411.

Bax, A., Clore, G.M., and Gronenborn, A.M. (1990). H-1-H-1 correlation via isotropic mixing of C-13 magnetization, a new 3-dimensional approach for assigning H-1 and C-13 spectra of C-13-enriched proteins. J. Magn. Reson. *88*, 425–431.

Birney, E., Kumar, S., and Krainer, A.R. (1993). Analysis of the RNA-recognition motif and RS and RGG domains: conservation in metazoan pre-mRNA splicing factors. Nucleic Acids Res. *21*, 5803–5816.

Black, D.L. (2003). Mechanisms of alternative pre-messenger RNA splicing. Annu. Rev. Biochem. *72*, 291–336.

Bothwell, A.L., Ballard, D.W., Philbrick, W.M., Lindwall, G., Maher, S.E., Bridgett, M.M., Jamison, S.F., and Garcia-Blanco, M.A. (1991). Murine polypyrimidine tract binding protein. Purification, cloning, and mapping of the RNA binding domain. J. Biol. Chem. *266*, 24657–24663.

Chan, R., and Black, D. (1997). The polypyrimidine tract binding protein binds upstream of neural cell specific c-src exon N1 to repress the spliciing of the intron downstream. Mol. Cell. Biol. *17*, 4667–4676.

Charlet, B.N., Logan, P., Singh, G., and Cooper, T.A. (2002). Dynamic antagonism between ETR-3 and PTB regulates cell type-specific alternative splicing. Mol. Cell *9*, 649–658.

Chou, M.Y., Underwood, J.G., Nikolic, J., Luu, M.H., and Black, D.L. (2000). Multisite RNA binding and release of polypyrimidine tract binding protein during the regulation of c-src neural-specific splicing. Mol. Cell *5*, 949–957.

Conte, M.R., Grüne, T., Ghuman, J., Kelly, G., Ladas, A., Matthews, S., and Curry, S. (2000). Structure of tandem RNA recognition motifs from polypyrimidine tract binding protein reveals novel features of the RRM fold. EMBO J. *19*, 3132–3141.

Cornilescu, G., Delaglio, F., and Bax, A. (1999). Protein backbone angle restraints from searching a database for chemical shift and sequence homology. J. Biomol. NMR *13*, 289–302.

Cote, C.A., Gautreau, D., Denegre, J.M., Kress, T.L., Terry, N.A., and Mowry, K.L. (1999). A *Xenopus* protein related to hnRNP I has a role in cytoplasmic RNA localization. Mol. Cell *4*, 431–437.

Delaglio, F., Grzesiek, S., Vuister, G.W., Zhu, G., Pfeifer, J., and Bax, A. (1995). NMRPipe: a multidimensional spectral processing system based on Unix pipes. J. Biomol. NMR *6*, 277–293.

Farrow, N.A., Muhandiram, R., Singer, A.U., Pascal, S.M., Kay, C.M., Gish, G., Shoelson, S.E., Pawson, T., Formankay, J.D., and Kay, L.E. (1994). Backbone dynamics of a free and a phosphopeptide-complexed Src homology-2 domain studied by N-15 NMR relaxation. Biochemistry *33*, 5984–6003.

Feigin, L.A., and Svergun, D.I. (1987). Structure Analysis by Small-Angle X-Ray and Neutron Scattering (New York: Plenum Press).

Gooding, C., Kemp, P., and Smith, C.W. (2003). A novel polypyrimidine tract-binding protein paralog expressed in smooth muscle cells. J. Biol. Chem. *278*, 15201–15207.

Gromak, N., Matlin, A.J., Cooper, T.A., and Smith, C.W. (2003a). Antagonistic regulation of alpha-actinin alternative splicing by CELF proteins and polypyrimidine tract binding protein. RNA *9*, 443–456.

Gromak, N., Rideau, A., Southby, J., Scadden, A.D., Gooding, C., Huttelmaier, S., Singer, R.H., and Smith, C.W. (2003b). The PTB interacting protein raver1 regulates alpha-tropomyosin alternative splicing. EMBO J. *22*, 6356–6364.

Hamilton, B.J., Genin, A., Cron, R.Q., and Rigby, W.F. (2003). Delineation of a novel pathway that regulates CD154 (CD40 ligand) expression. Mol. Cell. Biol. *23*, 510–525.

Handa, N., Nureki, O., Kurimoto, K., Kim, I., Sakamoto, H., Shimura, Y., Muto, Y., and Yokoyama, S. (1999). Structural basis for recognition of the tra mRNA precursor by the Sex-lethal protein. Nature *398*, 579–585.

Hellen, C.U.T., Witherall, G.W., Schmid, M., Shin, S.H., Pestova, T.V., Gil, A., and Wimmer, E. (1993). A cytoplasmic 57-kDa protein is required for translation of picornavirus RNA by internal ribosomal entry is identical to the nuclear pyrimidine tract-binding protein. Proc. Natl. Acad. Sci. USA *90*, 7642–7646.

Hunt, S.L., and Jackson, R.J. (1999). Polypyrimidine-tract binding protein (PTB) is necessary, but not sufficient, for efficient internal initiation of translation of human rhinovirus-2 RNA. RNA *5*, 344–359.

Johnson, B.A., and Blevins, R.A. (1994). NMRView: a computer-program for the visualization and analysis of NMR data. J. Biomol. NMR *4*, 603–614.

Kaminski, A., and Jackson, R.J. (1998). The polypyrimidine tract binding protein (PTB) requirement for internal initiation of translation of cardiovirus RNAs is conditional rather than absolute. RNA *4*, 626–638.

Kaminski, A., Belsham, G.J., and Jackson, R.J. (1994). Translation of encephaolmyocarditis virus RNA: parameters influencing the selection of the internal initiation site. EMBO J. *13*, 1673–1681.

Kaminski, A., Hunt, S.L., Patton, J.G., and Jackson, R.J. (1995). Direct evidence that polypyrimidine tract binding protein (PTB) is essential for internal initiation of translation of encephalomyocarditis virus RNA. RNA *1*, 928–938.

Kay, L.E., Torchia, D.A., and Bax, A. (1989). Backbone dynamics of proteins as studied by N-15 inverse detected heteronuclear nmr-spectroscopy—application to staphylococcal nuclease. Biochemistry *28*, 8972–8979.

Knoch, K.P., Bergert, H., Borgonovo, B., Saeger, H.D., Altkruger, A., Verkade, P., and Solimena, M. (2004). Polypyrimidine tract-binding protein promotes insulin secretory granule biogenesis. Nat. Cell Biol. *6*, 8–214.

Kolupaeva, V.G., Hellen, C.U.T., and Shatsky, I.N. (1996). Structural analysis of the interaction of the pyrimidine tract-binding protein with the internal ribosomal entry site of encephalomyocarditis virus and foot-and-mouth disease virus RNAs. RNA *2*, 1199–1212.

Konarev, P.V., Petoukhov, M.V., and Svergun, D.I. (2001). MASSHA: a graphic system for rigid body modelling of macromolecular complexes against solution scattering data. J. Appl. Crystallogr. *34*, 527–532.

Konarev, P.V., Volkov, V.V., Sokolova, A.V., Koch, M.H.J., and Svergun, D.I. (2003). PRIMUS: a Windows-PC based system for small-angle scattering data analysis. J. Appl. Crystallogr. *36*, 1277–1282.

Laskowski, R.A., Rullmannn, J.A., MacArthur, M.W., Kaptein, R., and Thornton, J.M. (1996). AQUA and PROCHECK-NMR: programs for checking the quality of protein structures solved by NMR. J. Biomol. NMR *8*, 477–486.

Laue, T. (2001). Biophysical studies by ultracentrifugation. Curr. Opin. Struct. Biol. *11*, 579–583.

le Maire, M., Rivas, E., and Moller, J.V. (1980). Use of gel chromatography for determination of size and molecular weight of proteins: further caution. Anal. Biochem. *106*, 12–21.

Li, B., and Yen, T.S. (2002). Characterization of the nuclear export signal of polypyrimidine tract-binding protein. J. Biol. Chem. *277*, 10306–10314.

Liu, H., Zhang, W., Reed, R.B., Liu, W., and Grabowski, P.J. (2002). Mutations in RRM4 uncouple the splicing repression and RNA-binding activities of polypyrimidine tract binding protein. RNA *8*, 137–149.

Lou, H., Helfman, D.M., Gagel, R.F., and Berget, S.M. (1999). Polypyrimidine tract-binding protein positively regulates inclusion of an alternative 3′-terminal exon. Mol. Cell. Biol. *19*, 78–85.

Maniatis, T., and Tasic, B. (2002). Alternative pre-mRNA splicing and proteome expansion in metazoans. Nature *418*, 236–243.

Mitchell, S.A., Spriggs, K.A., Coldwell, M.J., Jackson, R.J., and Willis, A.E. (2003). The Apaf-1 internal ribosome entry segment attains the

correct structural conformation for function via interactions with PTB and unr. Mol. Cell *11*, 757–771.

Moreira, A., Takagaki, Y., Brackenridge, S., Wollerton, M., Manley, J.L., and Proudfoot, N.J. (1998). The upstream sequence element of the C2 complement poly(A) signal activates mRNA 3′ end formation by two distinct mechanisms. Genes Dev. *12*, 2522–2534.

Mulligan, G.J., Guo, W., Wormsley, S., and Helfman, D.M. (1992). Polypyrimidine tract binding protein interacts with sequences involved in alternative splicing of beta-tropomyosin pre-mRNA. J. Biol. Chem. *267*, 25480–25487.

Oh, Y.L., Hahm, B., Kim, Y.K., Lee, H.K., Lee, J.W., Song, O.-K., Tsukiyama-Kohara, K., Kohara, M., Nomoto, A., and Jang, S.K. (1998). Determination of functional domains in polypyrimidine-tract binding protein. Biochem. J. *331*, 169–175.

Oubridge, C., Ito, N., Evans, P.R., Teo, C.H., and Nagai, K. (1994). Crystal structure at 1.92 Å resolution of the RNA-binding domain of the U1A spliceosomal protein complexed with an RNA hairpin. Nature *372*, 432–438.

Pérez, I., Lin, C.H., McAfee, J.G., and Patton, J.G. (1997a). Mutation of PTB binding sites causes misregulation of alternative 3′ splice site selection in vivo. RNA *3*, 764–778.

Pérez, I., McAfee, J.G., and Patton, J.G. (1997b). Multiple RRMs contribute to RNA binding specificity and affinity for polypyrimidine tract binding protein. Biochemistry *36*, 11881–11890.

Pilipenko, E.V., Viktorova, E.G., Guest, S.T., Agol, V.I., and Roos, R.P. (2001). Cell-specific proteins regulate viral RNA translation and virus-induced disease. EMBO J. *20*, 6899–6908.

Roberts, G.C., and Smith, C.W. (2002). Alternative splicing: combinatorial output from the genome. Curr. Opin. Chem. Biol. *6*, 375–383.

Schwieters, C.D., Kuszewski, J.J., Tjandra, N., and Clore, G.M. (2003). The Xplor-NIH NMR molecular structure determination package. J. Magn. Reson. *160*, 65–73.

Simpson, P.J., Davydova, N., Curry, S., and Matthews, S. (2002). Resonance assignment and topology of the 2H, 13C, 15N labelled 29 kDa N-terminal fragment of the polypyrimidine tract binding protein (PTB). J. Biomol. NMR *24*, 79–80.

Singh, R., Valcárcel, J., and Green, M.R. (1995). Distinct binding specificities and functions of higher eukaryotic polypyrimidine tract-binding proteins. Science *268*, 1173–1176.

Southby, J., Gooding, C., and Smith, C.W.J. (1999). Polypyrimidine tract binding protein functions as a repressor to regulate alternative splicing of α-actinin mutually exclusive exons. Mol. Cell. Biol. *19*, 2699–2711.

Svergun, D.I. (1992). Determination of the regularization parameter in indirect transform methods using perceptual criteria. J. Appl. Crystallogr. *25*, 495–503.

Svergun, D.I. (1993). A direct indirect method of small-angle scattering data treatment. J. Appl. Crystallogr. *26*, 258–267.

Svergun, D.I. (1999). Restoring low resolution structure of biological macromolecules from solution scattering using simulated annealing. Biophys. J. *76*, 2879–2886.

Tillmar, L., and Welsh, N. (2002). Hypoxia may increase rat insulin mRNA levels by promoting binding of the polypyrimidine tract-binding protein (PTB) to the pyrimidine-rich insulin mRNA 3′-untranslated region. Mol. Med. *8*, 263–272.

Wagner, E.J., and Garcia-Blanco, M.A. (2001). Polypyrimidine tract binding protein antagonizes exon definition. Mol. Cell. Biol. *21*, 3281–3288.

Williamson, R.A., Carr, M.D., Frenkiel, T.A., Feeney, J., and Freedman, R.B. (1997). Mapping the binding site for matrix metalloproteinase on the N-terminal domain of the tissue inhibitor of metalloproteinases-2 by NMR chemical shift perturbation. Biochemistry *36*, 13882–13889.

Wishart, D.S., Sykes, B.D., and Richards, F.M. (1991). Relationship between nuclear-magnetic-resonance chemical-shift and protein secondary structure. J. Mol. Biol. *222*, 311–333.

Wollerton, M.C., Gooding, C., Wagner, E.J., Garcia-Blanco, M.A., and Smith, C.W. (2004). Autoregulation of polypyrimidine tract binding protein by alternative splicing leading to nonsense-mediated decay. Mol. Cell *13*, 91–100.

Xu, R.M., Jokhan, L., Xiaodong, G., Mayeda, A., and Krainer, A. (1997). Crystal structure of human UP1, the domain of hnRNP A1 that contains two RNA-recognition motifs. Structure *5*, 559–570.

Yamazaki, T., Formankay, J.D., and Kay, L.E. (1993). 2-dimensional NMR experiments for correlating C-13-beta and H-1-delta/epsilon chemical-shifts of aromatic residues in C-13-labeled proteins via scalar couplings. J. Am. Chem. Soc. *115*, 11054–11055.

Yuan, X., Davydova, N., Conte, M.R., Curry, S., and Matthews, S. (2002). Chemical shift mapping of RNA interactions with the polypyrimidine tract binding protein. Nucleic Acids Res. *30*, 456–462.

Zhang, L., Liu, W., and Grabowski, P.J. (1999). Coordinate repression of a trio of neuron-specific splicing events by the splicing regulator PTB. RNA *5*, 117–130.

Accession Numbers

Structural coordinates for PTB1-1 and PTB2-2 have been deposited in the PDB under ID codes 1SJQ and 1SJR, respectively.